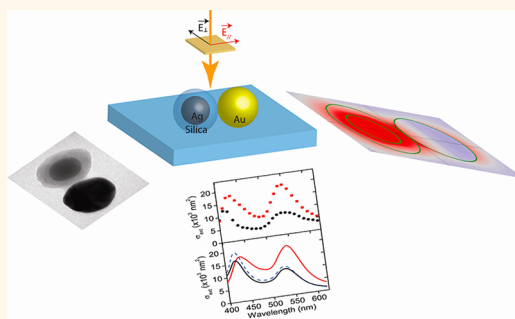# Optical Response of Individual Au−Ag@SiO₂ Heterodimers

Anna Lombardi,[†] Marcin P. Grzelczak,[‡] Aurélien Crut,[†,*] Paolo Maioli,[†] Isabel Pastoriza-Santos,[‡] Luis M. Liz-Marzán,[‡,§,⊥] Natalia Del Fatti,[†] and Fabrice Vallée[†]

[†]FemtoNanoOptics Group, Institut Lumière Matière UMR5306, Université Lyon 1-CNRS, 69622 Villeurbanne, France, [‡]Departamento de Química Física, Universidade de Vigo, 36310 Vigo, Spain, [§]Bionanoplasmonics Laboratory, CIC biomaGUNE, Paseo de Miramón 182, 20009 Donostia-San Sebastián, Spain, and [⊥]Ikerbasque, Basque Foundation for Science, 48011 Bilbao, Spain

ABSTRACT The optical extinction response of individual Au−Ag@SiO₂ heterodimers whose individual morphologies are determined by transmission electron microscopy (TEM) is investigated using spatial modulation spectroscopy. The extinction spectra show two resonances spectrally close to the surface plasmon resonances of the constituting Au and Ag@SiO₂ core−shell particles. The interparticle electromagnetic coupling is demonstrated to induce a large increase of the optical extinction of the dimer around its Au-like surface plasmon resonance for light polarized along its axis, as compared to that for perpendicular polarization and to that of an isolated Au nanoparticle. For spherical particles, this interaction also leads to comparable shifts with light polarization of the two dimer resonances, an effect masked or even reversed for particles significantly deviating from sphericity. Both amplitude and spectral effects are found to be in excellent quantitative agreement with numerical simulations when using the TEM-measured dimer morphology (*i.e.*, size, shape, and orientation of the individual dimers), stressing the importance of individual morphology characterization for interpreting heterodimer optical response.

KEYWORDS: single-particle absorption · heterodimers · plasmonic interactions · noble metals · Fano resonance · finite-element modeling

The optical response and the concomitant local field enhancement effect associated with the localized surface plasmon resonance (LSPR) of metal nano-objects have been extensively investigated, both experimentally and theoretically, during the past decade. Though the LSPR spectral position, amplitude, and light polarization dependence can be modified and optimized for specific applications through tuning of the nano-object size, shape, and composition,[1,2] possibilities are limited when using objects formed by a single particle. This limitation is particularly important for applications requiring large local enhancement of the electromagnetic field in and around the nano-object. In this context, plasmonic coupling between two (or more) interacting metal nanoparticles forming a nano-object offers many new possibilities for tailoring its optical response, as well as the amplitude and spatial distribution of the associated local field.[3,4] Homodimers formed by two interacting particles of the same metal have

been synthesized and investigated,[5−11] and their optical response has been qualitatively interpreted in the context of the plasmon hybridization model[8,12,13] and reproduced using numerical simulations.[8,9,14,15] In particular, the effect of size or shape asymmetry (using gold nanosphere−nanoshell dimers) of the forming nanoparticles has also been investigated.[8,10,11] The concomitant large field enhancement between the constituting particles has been exploited to enhance Raman scattering[16] or fluorescence[17] of molecules or to create high-sensitivity sensors,[18,19] and the optical response dependence on the interparticle distance is used to develop "plasmon rulers".[7,20,21]

Although they offer even larger versatility, heterodimers constituted by two nanoparticles of different metals have been much less investigated, mainly because of the difficulty involved in their controlled fabrication. In the case of model systems formed by interacting Au and Ag nanospheres, the numerically computed spectra

© 2013 American Chemical Society

show two resonances, with wavelengths close to those of the LSPR of isolated Ag and Au spheres.[10,22−25] Their electromagnetic coupling leads to a large enhancement of the computed optical response (absorption or scattering) around the Au-like LSPR when the light polarization is changed from orthogonal to parallel with respect to the dimer axis and as compared to that of the isolated Au particle. Concomitantly, a small red shift of both resonances is predicted, in contrast to the prediction of the plasmon hybridization model, which neglects coupling between the LSPR and the continuum of interband transitions[10,22−25] (the red shift of the Ag-like LSPR originating from the Fano profile of gold nanoparticle absorption in a Ag−Au dimer[22,25]). The latter spectral signature has been recently observed by measuring the optical scattering spectra of individual heterodimers formed by gold and silver nanospheres linked by a DNA chain.[10] However, the spectral shape (*e.g.*, the relative amplitude of the resonances) and light polarization dependence of the scattering amplitude of the studied dimers were found to be very different from the computed ones assuming the dimer is formed by nanospheres. This suggests that the observed polarization dependence of the measured spectra is not only due to plasmon hybridization but also reflects other effects such as deviation from sphericity of the forming particles and/or oxidation issues (see below).

To fully and unambiguously analyze the optical response of heterodimers, we have investigated differently synthesized nano-objects formed by a gold particle bound to a silica-coated silver particle (Au−Ag@SiO$_2$ dimers). The silica shell of the Ag@SiO$_2$ particle permits both controlling the distance separating the gold and silver components and (importantly) preventing silver oxidation. The optical extinction spectra of individual dimers were measured using spatial modulation spectroscopy, a technique that has the advantage of providing absolute cross-section measurements, conversely to more commonly used dark-field microspectroscopy techniques. Transmission electron microscopy (TEM) was then used to determine the individual morphology of each optically investigated nanodimer. This correlation is particularly important here, as the optical signatures of electromagnetic coupling in a dimer of nanospheres can be significantly altered, or even suppressed, when the forming particles deviate from sphericity. Excellent agreement was obtained between the experimental spectral features, amplitudes, and light polarization dependence of the extinction cross-sections of different single heterodimers and the results of numerical simulations using their measured morphology as an input. Qualitative agreement was also obtained with generalization of the dipolar hybridization model[10] taking into account the gold interband transitions, *i.e.*, the valence electrons.

EXPERIMENTAL RESULTS AND DISCUSSION

Experiments were performed on model colloidal heterodimers formed by a gold nanosphere bound to a core−shell Ag@SiO$_2$ nanoparticle (Figure 1a). The dimers were synthesized by first independently preparing solutions of gold nanospheres in ethanol and silica-coated silver nanoparticles in water (see Methods). Although the selected synthesis of silver nanoparticles[26] yields mostly nanocubes, a significant amount of spheres was also formed, which were selected for the subsequent measurements. Additional reshaping may also occur during the silica coating process, even though the base catalyst was dimethylamine rather than ammonia,[27] and thus the sol−gel reaction medium was significantly less oxidizing. The binding between the components of the dimer was achieved through surface modification of the Ag@SiO$_2$ particles with a positively charged polyelectrolyte (poly(allylamine hydrochloride), PAH), which can readily
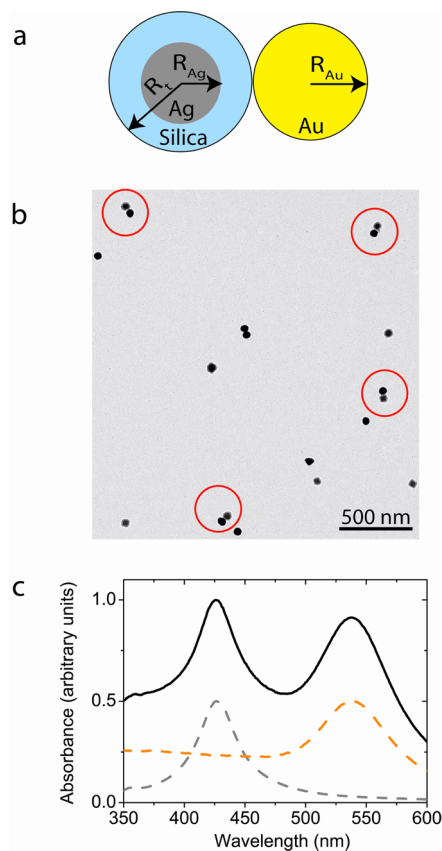

Figure 1. a) Model morphology of an Au−Ag@SiO$_2$ heterodimer formed by spherical particles. b) TEM image of nanoparticles of the Au−Ag@SiO$_2$ solution showing the presence of heterodimers (indicated by red circles) and of unpaired particles. c) Normalized absorbance of one of the synthesized Au−Ag@SiO$_2$ solutions (plain black line) and of the initial Ag@SiO$_2$ (dashed grey line) and Au (dashed orange line) nanoparticle solutions (these last spectra were normalized to a maximum value of 0.5 for clarity). The mean size of the Au particle is $\langle R_{Au} \rangle$ = 32.5 nm, and that of the Ag core $\langle R_{Ag} \rangle$ = 18.5 nm with a SiO$_2$ shell thickness $\langle R_t - R_{Ag} \rangle$ = 16 nm.

bind to the gold nanoparticles, which are weakly negatively charged upon ligand exchange and coating with poly(vinylpyrrolidone) (PVP). Heterodimers were then formed by electrostatic assembly of Ag@SiO$_2$@PAH and Au@PVP nanoparticles when mixing the solutions. After incubation for 2 h to allow electrostatic attachment, the sample was centrifuged at low speed (1100 rpm) to remove part of the unbound nanoparticles. The precipitate was redispersed in water and found to contain a high concentration of heterodimers (about one-third of the particles present in the solution), as shown by TEM characterization (Figure 1b). The gold particles have a larger average size than the silver cores of the Ag@SiO$_2$ particles in order to increase their relative contribution to the optical response of the dimer (the LSPR amplitude being smaller for gold than for silver nanospheres of identical sizes, because of LSPR interband damping in gold).[25,28] The shell thickness of the Ag@SiO$_2$ particles was chosen to be smaller than the Au and Ag sizes to permit sufficient Au−Ag electromagnetic coupling, a nanosphere being sensitive to its environment over a distance of typically its size.[29] For the synthesized particles, TEM characterizations yield an average Au diameter of 65 nm and, for the core−shell Ag@SiO$_2$ particles, an average Ag core size of 37 nm covered by a silica shell with 16 nm average thickness.

As expected, the absorption spectrum of the colloidal solution of heterodimers exhibits two resonances around 430 and 540 nm (full line in Figure 1c). Their spectral positions are almost identical to those observed for the LSPR of the initial solutions of Ag@SiO$_2$ and gold nanoparticles, respectively (dashed lines in Figure 1c). As dimer formation is expected to mostly show up in amplitude- and polarization-dependent changes in the optical spectrum,[10,22−25] these effects are difficult to observe in ensemble measurements due to the presence of unpaired particles and to random dimer orientation (Figure 1b). These drawbacks are suppressed by investigating individual nano-objects, which permits us to address their polarization-dependent optical response.[30] The spectra and absolute values of the extinction cross-section of individual heterodimers were measured using the spatial modulation spectroscopy (SMS) technique.[31] This relies on modulation at frequency f of the position of a nano-object in the focal spot of a tightly focused light beam of wavelength λ (Figure 2a). The presence of a nano-object results in modulation of the transmitted light power, with an amplitude proportional to its extinction cross-section $\sigma_{ext}(\lambda)$ and sum of its absorption (σ_{abs}) and scattering (σ_{scat}) cross-sections. After calibrating the focal spot size and modulation amplitude, the absolute value of $\sigma_{ext}(\lambda)$ can be determined. In our experiments, $\sigma_{ext}(\lambda)$ was measured in the 400−650 nm range using a tunable light source formed by a femtosecond optical parametric oscillator system and a frequency-doubled femtosecond Ti:Sapphire oscillator
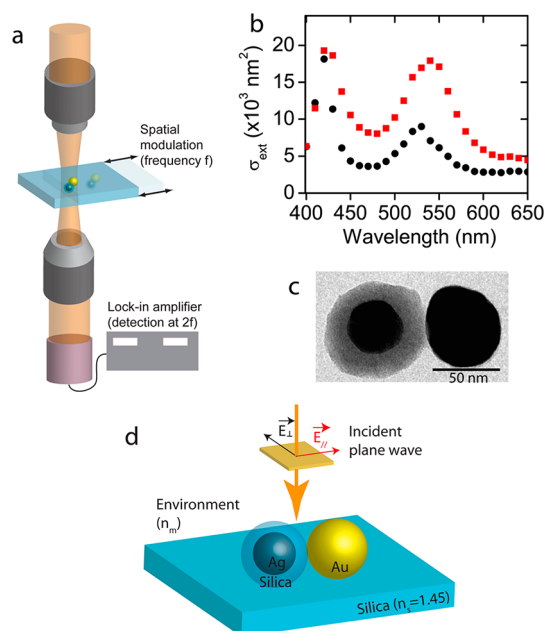

Figure 2. (a) Principle of spatial modulation spectroscopy (SMS) setup for measurement of the extinction cross-section of individual nano-objects. (b) Extinction spectra of a single Au−Ag@SiO$_2$ heterodimer deposited on a thin silica layer supported by a TEM grid, for incident light polarization parallel (red squares) and orthogonal (black circles) to the dimer axis. (c) TEM image of the investigated dimer formed by quasispherical particles with R_{Au} = 29 nm, R_{Ag} = 20 nm, and a SiO$_2$ shell thickness $R_t − R_{Ag}$ = 16 nm (Figure 1a). (d) Model of Au−Ag@SiO$_2$ heterodimer deposited on a glass substrate used in FEM computations in the case of spherical nanoparticles.

(see Methods). The incident light was linearly polarized, and its polarization direction controlled using the combination of a quarter-wave plate and a polarizer. Due to the limited spatial resolution of far-field techniques, SMS measurements can be performed only on samples with a low surface density of particles (less than about one particle per μm^2). These were prepared by spin-coating the Au−Ag@SiO$_2$ heterodimer solution on a substrate compatible with TEM measurements (i.e., TEM grids covered by a 40 nm thick silica film; see Methods). This approach permits combining optical spectroscopy of an individual nanoparticle and determination of its morphology and orientation by TEM.[32−35]

The measured extinction spectrum of an Au−Ag@SiO$_2$ dimer formed by quasispherical particles is illustrated in Figure 2b for linearly polarized light, with polarization either along or perpendicular to its axis. This relative orientation was determined observing the dimer orientation on the substrate, together with its morphology, by TEM imaging (Figure 2c) and used in the modeling (Figure 2d, see below). As the ensemble spectrum (Figure 1c), the σ_{ext} spectrum of a single heterodimer exhibits two resonances with central wavelengths around 420 and 530 nm. However, the spectral positions were found to shift when the light
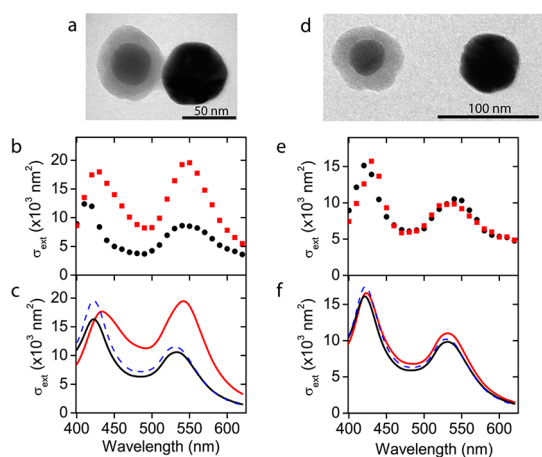
Figure 3. (a) TEM image and (b) extinction cross-section spectra of the same Au−Ag@SiO₂ heterodimer for incident light polarized parallel (red squares) and orthogonal (black circles) to the dimer axis. (c) Computed extinction cross-section spectra for parallel (red line) and orthogonal (black line) polarizations for spherical constituting particles with the TEM measured sizes: R_{Au} = 29 nm, R_{Ag} = 19 nm, and R_t = 33 nm. The dashed line is the sum of the computed extinction cross-sections of isolated Au and Ag@SiO₂ nanospheres with the same sizes. (d−f) The same information for a pair of separated quasispherical Ag@SiO₂ and Au particles, with R_{Au} = 28 nm, R_{Ag} = 18 nm, R_t = 35 nm, and a 50 nm surface to surface separation between the two nanoparticles. A mean refractive index of the environment above the substrate n_m = 1.3 was used in both FEM simulations.

Figure 4. Same as Figure 3 in the case of heterodimers formed by nonspherical particles. The heterodimer in the left column is formed by an almost spherical Au nanoparticle of radius R_{Au} = 28 nm and by a Ag@SiO₂ particle elongated along a direction almost perpendicular to the dimer axis. The Ag particle is modeled as a prolate ellipsoid with long axis of 59 nm and a short axis of 50 nm (i.e., an aspect ratio of 1.2). Conversely the Ag@SiO₂ particle forming the heterodimer in the right column is almost spherical, with R_{Ag} = 26 nm and R_t = 37 nm, while the Au particle is elongated and has been modeled as a prolate ellipsoid with long axis of 66 nm and a short axis of 50 nm (i.e., an aspect ratio of 1.3). The dashed lines are the sum of the computed extinction cross-sections of isolated Au and Ag@SiO₂ nanoparticles with the same sizes for the two orthogonal light polarizations. A mean refractive index of the environment above the substrate n_m = 1.25 was used in both FEM simulations.

polarization direction was changed, with extrema corresponding to polarization either parallel or perpendicular to the dimer axis. For the latter polarization, the resonances are close to those of the LSPR of a silver sphere in silica (about 420 nm) and of a gold sphere deposited on a glass substrate (about 530 nm).[29,36] Both resonances are shifted by ∼10 nm to longer wavelengths for parallel polarization. The most striking effect of polarization is however on the σ_{ext} amplitude, which gets enhanced mostly around the Au-like resonance. In this spectral region, the peak σ_{ext} amplitude is about two times larger for parallel than for orthogonal polarization, while it is comparable for both polarization directions around the Ag-like resonance (Figures 2b and 3b). These spectral and amplitude polarization dependencies are consistent with those computed for significant electromagnetic coupling between gold and silver nanospheres.[10,22−25] However, the above spectral signature (i.e., red shift of both resonances for light polarized along the dimer axis as compared to perpendicular polarization) is observed only when the heterodimer is formed by almost spherical nanoparticles. Modified or even reversed behavior can be observed when the constituent particles significantly deviate from sphericity, as illustrated in Figure 4 (see full discussion below).

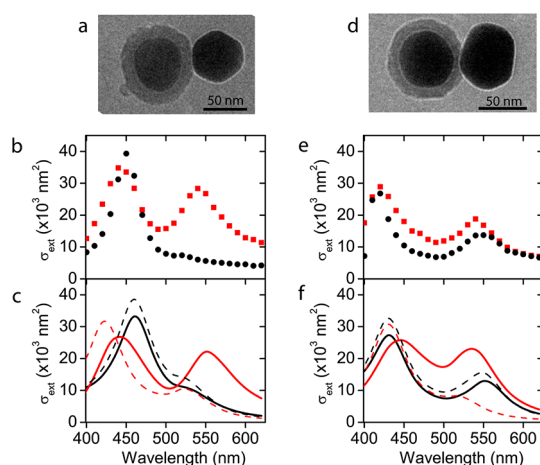To interpret these combined effects in the heterodimer responses, a more detailed analysis was carried out here as the morphology of each optically investigated dimer is known from TEM imaging. Numerical simulations of the optical extinction spectra were performed using finite element modeling (FEM) with a classical approach based on Maxwell's equations and the material dielectric functions. Dimers formed by quasispherical nanoparticles were modeled as a gold sphere of radius R_{Au} in contact with a silica-coated silver sphere with core and external radius R_{Ag} and R_t, respectively (Figure 1a). The different sizes were determined from TEM images (Figures 2c and 3a). The dielectric constants reported by Johnson and Christy[37] and Palik[38] were used for gold and silver, respectively, as they permit good reproduction of the LSPR wavelength of single metal nanoparticles.[29,36,39,40] Corrections for size effects were neglected, as they only yield minor broadening of the LSPR for the relatively large sizes of the component particles used here.[36,41] The presence of the substrate was taken into account assuming it occupies the semi-infinite space below the nano-object (Figure 2d).[34,35] In this modeling, the only free parameter is the refractive index, n_m, of the mean environment embedding the nano-object above the substrate. It can significantly deviate from the air value due to the presence of surfactant molecules and of residual solvent, as shown in previous studies using similar experimental geometry.[34,35] Here, n_m values in the 1.2−1.3 range were typically used to reproduce the spectral position of the dimer resonances.

The spectral shape and amplitudes of the computed σ_{ext} spectra are in excellent quantitative agreement with the experimental ones for quasispherical particles (Figure 3c,f). In particular, the wavelength and relative amplitude of the resonances, as well as their light polarization dependence, are well predicted. To confirm the origin of the polarization dependence of the σ_{ext} spectra, measurements on a pair of separated Au nanosphere and Ag@SiO$_2$ nanoparticle with almost spherical cores have been performed. This pair, randomly formed during the spin-coating process, was identified by TEM imaging (Figure 3d). The interparticle distance, about 50 nm from surface to surface, is comparable to their size, making them only very weakly interacting. As expected, the measured extinction spectrum is then almost independent of light polarization, with basically identical amplitudes for both polarizations and only minor spectral shifts (Figure 3e). This behavior is in stark contrast with that observed for all the investigated Au−Ag@SiO$_2$ heterodimers formed by almost spherical particles (Figure 2c and Figure 3a), thereby confirming their large electromagnetic coupling for parallel as compared to perpendicular polarization. In the case of the pair of distant nanoparticles, the σ_{ext} spectra are almost identical to the sum of the computed ones for the constituting Au and Ag@SiO$_2$ nanoparticles (Figure 3f), as expected, because of their weak electromagnetic coupling due to their large separation. In contrast, for a heterodimer the σ_{ext} spectrum is close to that of the sum of the constituent particles only for orthogonal polarization (with almost no spectral shift, and only reduction of σ_{ext} around the Ag-like LSPR, Figure 3c). It strongly deviates from that for parallel polarization, showing a red shift of both resonances and an increase of the σ_{ext} amplitude around the Au-like LSPR, in quantitative agreement with the experimental results (Figure 3e,f).

The dependence of σ_{ext} on Au−Ag separating distance was investigated using FEM modeling, by performing calculations similar to those leading to Figure 3c, for various values of the silica shell thickness (Figure S1 in the Supporting Information). The results show that electromagnetic coupling effects on the extinction spectra (i.e., LSPR amplitude changes and position shifts) monotonically increase with decreasing distance. However, these variations remain moderate in the thickness range that is accessible with our synthesis protocol (typically 10−50 nm silica shell thickness). Investigation of the near-touching regime, for which large modifications of LSPR amplitude and position as well as nonclassical effects are expected,[42] would require the development of a new synthesis method for coating silver nanoparticles with thinner silica shells, which is out of the scope of this paper (note that gold encapsulation with a thin silica shell has been demonstrated,[43,44] but investigation of Ag−Au@SiO$_2$ would raise the important issue of silver oxidation).

For a quasispherical Au particle and a slightly elongated Ag particle (Figure 4a), the Au-like LSPR exhibits the expected red shift with parallel light polarization, while in contrast, a blue shift is observed for the Ag-like LSPR (Figure 4b). The opposite behavior is observed for a dimer formed by an elongated Au particle and an almost spherical Ag particle (Figure 4d,e). These opposite wavelength shifts of the Au and Ag-like LSPRs are ascribed to overcompensation of the effect due to Au−Ag particle interaction by that due to the particle shape anisotropy (the LSPR of an elongated particle being red-shifted for light polarized along its long axis as compared to its short one). In both cases, enhancement of the σ_{ext} amplitude around the Au-like LSPR for parallel polarization is observed. However, the observed enhancement depends on the particle size and shape and is particularly large in the case of the dimer of Figure 4a (4-fold enhancement of σ_{ext} at 540 nm). To analyze the impact of the shape anisotropy and relative size of the constituting nanoparticles on the measured spectra, similar FEM calculations were performed for heterodimers formed by elongated particles. Following the TEM-measured morphology shown in Figure 4, one of the particles was assumed to be spherical and, as a first approximation, the shape of the other one was modeled as a prolate ellipsoid (the Ag particle in Figure 4a and the Au particle in Figure 4d, with aspect ratios of about 1.2 and 1.3, respectively) with a long axis orthogonal to that of the dimer. The polarization dependencies of the spectral positions of the resonances of the two heterodimers are very well reproduced (Figure 4). In particular, in the case of an elongated Ag nanoparticle, the Ag-like LSPR for orthogonal polarization (parallel to the long nanoparticle axis) is red-shifted as compared to parallel polarization, showing that shape anisotropy effect dominates over the one due to electromagnetic coupling (Figure 4b). A similar effect is observed for the elongated Au nanoparticle close to the Au-like LSPR of the dimer (Figure 4e). These observed spectral shifts of the Au- and Ag-like LSPRs, in excellent agreement with numerical simulations (Figure 4c,f), are in contrast to those calculated and observed in the case of spherical particles, though relatively small particle anisotropies are considered. This stresses the importance of particle anisotropy on the observed optical response of a dimer and, thus, the necessity of precisely determining its morphology. The amplitude of the σ_{ext} spectrum and its polarization dependence are also very well reproduced, showing that when the dimer is constituted by Ag and Au nanoparticles with similar sizes (Figure 4a), the weak Au-like LSPR observed for perpendicular light polarization is strongly enhanced for parallel polarization (factor of 4) due to interaction with the Ag particle. Other orientations of the elliptical particles are discussed in the Supporting Information (numerical simulations in Figure S2 and experiments in Figure S3). This further
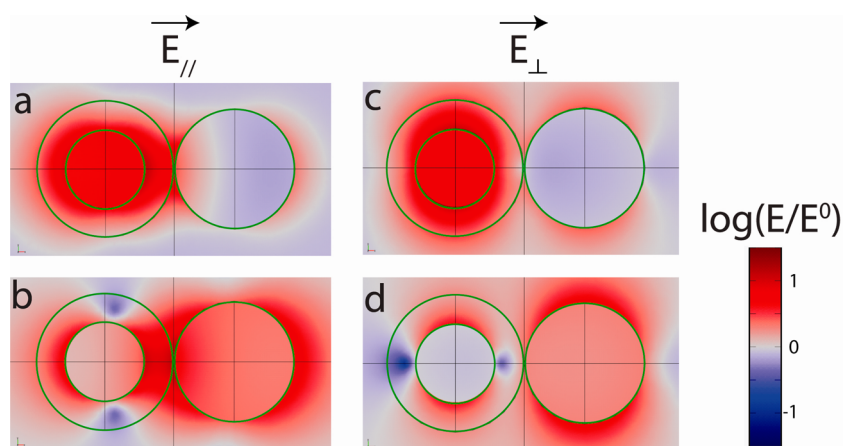
Figure 5. Spatial distribution of the total electric field in and around the Au−Ag@SiO$_2$ heterodimer of Figure 3a, formed by spherical particles with R_{Au} = 29 nm, R_{Ag} = 19 nm, and R_t = 33 nm, computed using FEM. The incident light polarization is parallel (a, b) and orthogonal (c, d) to the dimer axis, and the field is computed at σ_{ext} resonance wavelengths, as in Figure 3b: (a) 430 nm, (b) 540 nm, (c) 420 nm, and (d) 530 nm. The electric field amplitude is normalized to that of the incident wave (E^0) and shown on a color-coded logarithmic scale.

illustrates the strong dependence of spectral shifts on particle orientation, as well as the amplification of coupling effects when the elongation direction coincides with the dimer axis. The optical response of dimers involving nanoparticles with nonspheroidal shapes is also shown (*e.g.*, triangular shape, see Figure S3), their accurate modeling requiring even more precise determination of their morphology, using for instance 3D electron tomography.[45,46]

For the size of the nanoparticles shown in Figures 2 and 3, the absorption contribution to the extinction is typically two times larger than scattering (Figure S4 in the Supporting Information; for larger ones such as in Figure 4, scattering becomes comparable to absorption). The computed σ_{abs} and σ_{scat} spectral features are similar, and their polarization dependencies can be ascribed to variation of their electromagnetic coupling, *i.e.*, modification of the local field in one particle due to coupling with the other. This is illustrated by computing the electric field amplitude map of the electromagnetic field for the heterodimer of Figure 3, at its resonance wavelengths and for different polarization directions (Figure 5). For orthogonal polarization, the electric field distributions at the Ag-like and Au-like LSPRs (about 420 and 530 nm, respectively) are similar to those of noninteracting nanoparticles (presented in Figure S5, in the Supporting Information), which is consistent with observation of similar extinction spectra (Figure 3c). In contrast, for parallel polarization, electromagnetic coupling in the dimer creates a large field anisotropy, with large enhancements in the region between the particles.

As previously mentioned, the observed spectral behavior (*i.e.*, red shift of both resonances for interacting nanospheres) is in contrast to that predicted by the dipolar plasmon hybridization model in its simplest form (*i.e.*, describing interaction of two plasmonic resonances). Spectral separation of the resonances,

i.e., red and blue shifts of the long- and short-wavelength resonances, respectively, is then predicted for parallel polarization that maximizes the dipole−dipole interaction.[10,12,13] For heterodimers, resonant interaction of the LSPR with other states has to be included, *e.g.*, the continuum of gold interband transitions that overlaps the Ag-like LSPR.[10] This can be simply introduced by describing each forming particle as a polarizable entity with polarizability α calculated from its full dielectric constant, ε, and neglecting the spatial variation of the incident electromagnetic wave over the dimer (quasistatic approximation), assuming its size is much smaller than the optical wavelength. For an isolated spherical particle of radius R, $\alpha = 4\pi R^3(\varepsilon - \varepsilon_m)/(\varepsilon + 2\varepsilon_m)$ (where ε_m is the dielectric function of the embedding material, assumed to be homogeneous here), its induced dipole moment being proportional to the product of α and the external electric field. Conversely, the field experienced by a particle in a dimer is the sum of the external field plus that due to the dipole induced in the other particle. One can then calculate the dimer polarizability for perpendicular and parallel light polarization, respectively (details are provided in the text of the Supporting Information):

$$\alpha_{\parallel} = \frac{\alpha_{Ag} + \alpha_{Au} + \dfrac{\alpha_{Ag}\alpha_{Au}}{\pi l^3}}{1 - \dfrac{\alpha_{Ag}\alpha_{Au}}{(2\pi l^3)^2}} \qquad \alpha_{\perp} = \frac{\alpha_{Ag} + \alpha_{Au} - \dfrac{\alpha_{Ag}\alpha_{Au}}{2\pi l^3}}{1 - \dfrac{\alpha_{Ag}\alpha_{Au}}{(4\pi l^3)^2}} \quad (1)$$

where $\alpha_{Au,Ag}$ are the polarizabilities of the gold and silver particles, and l is the center-to-center distance of the spheres in the dimer. The dimer absorption and scattering cross-sections are then obtained from the imaginary part and square modulus of its polarizability, respectively (see Supporting Information). The cross-sections computed for the dimer morphology of Figure 3a are shown in Figures 6a and S6a for parallel and perpendicular polarizations, respectively. They are in qualitative agreement with those obtained with FEM, showing in
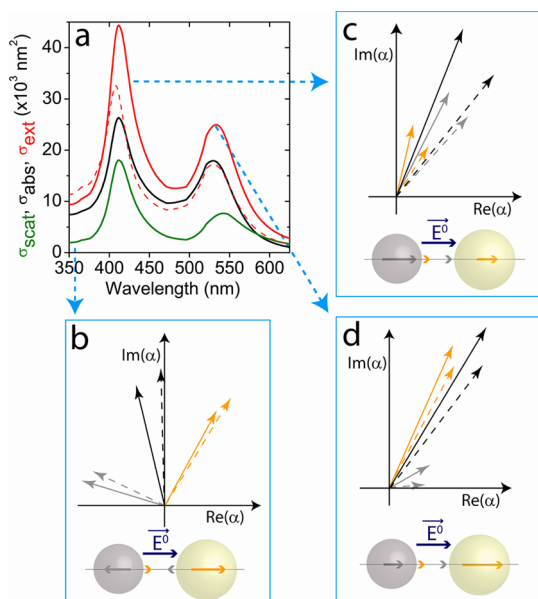
Figure 6. (a) Extinction, absorption, and scattering cross-sections (plain red, black, and green lines, respectively) computed using the dipolar-quasistatic model for incident light polarized parallel to the axis of a Ag−Au heterodimer formed by Ag and Au nanospheres of radius 19 and 29 nm, respectively (a homogeneous environment with a refractive index of 1.45 was assumed). The dashed line is the sum of the extinction cross-sections computed for isolated gold and silver nanospheres. (b−d) Complex polarizabilities computed at 360 nm (b), 420 nm (c), and 530 nm (d) for the dimer (plain black) and its silver and gold components (gray and orange arrows, respectively) and in absence of interaction (dashed lines). Situation (b) roughly corresponds to out-of-phase induced dipoles for the gold and silver spheres, while (c) and (d) correspond to similar phases.

particular the enhancement of the dimer optical response for light polarization parallel to its axis, as compared to the simple sum of the individual extinction spectra of the constituting nanoparticles (Figure 6). The quantitative amplitude and width of the silver-like resonance and its polarization dependence are however not correctly reproduced, probably because of neglecting multipolar effects and assuming an optically uniform environment around the gold and silver particles.

This dipolar-quasistatic model permits us to qualitatively interpret the general trends of the optical spectrum in terms of wavelength-dependent dipolar interaction of the component particles. Around the Au-like LSPR (at about 530 nm) and on the red side of the Ag-like LSPR, the field created by one particle at the position of the other particle is weakly dephased with respect to the external field, and therefore the two fields interfere constructively. This increases the induced dipolar amplitude and modifies its phase, as reflected in the effective polarizability of interacting Au and Ag particles, as compared to noninteracting ones (as demonstrated by the representation of polarizabilities in the complex plane shown in Figure 6c,d, where vector length and inclination with respect to the horizontal axis account for the polarizability amplitude

and dephasing with the external field, respectively; see also Supporting Information). The polarizability (full black arrow in Figure 6c,d) and the extinction cross-section of the dimer are thus enhanced as compared to those of a noninteracting pair (dashed black arrow in Figure 6c,d). On the blue side of the Ag-like LSPR, the polarizability of the Ag particle, dominated by its free electron response, is phase-shifted by almost $\pi/2$ as a result of the sign change of $\text{Re}(\varepsilon + 2\varepsilon_\text{m})$ at the Ag LSPR (Figure 6b).[22] This eventually reduces the dimer optical response as compared to that of the noninteracting pair, because of destructive interference between the external field and that scattered by the silver particle (Figure 6a around 360 nm). For orthogonal polarization, the polarizability of the constituting particles and of the dimer are very similar due to coupling reduction. For our dimer morphology, the spectrum is thus almost identical to the noninteracting particle one, in agreement with FEM modeling (Figure S6 of the Supporting Information).

CONCLUSION

The extinction spectrum and amplitude of individual Ag−Au heterodimers and their dependencies on light polarization have been investigated using spatial modulation spectroscopy. Experiments were performed on model systems formed by Au nanoparticles in contact with a core−shell Ag-SiO$_2$ particle, the silica shell acting as spacer and preventing silver oxidation. The measured extinction spectra are close to the sum of the extinction spectra of the isolated Au and Ag@SiO$_2$ particles for light polarized perpendicular to the dimer axis. In contrast, a large enhancement of the extinction cross-section around the gold-like LSPR is observed for light polarized along it, also in comparison to that of an isolated Au particle (by a factor of 1.5 to 4 for the investigated dimers, depending on the constituent particle sizes and shapes). This Au-like LSPR enhancement is the signature of strong electromagnetic coupling of the Ag and Au particles in the dimer, for parallel polarization. For spherical particles, this coupling also leads to red shifts of both the dimer resonances when changing the light polarization direction from perpendicular to parallel to the dimer axis. This polarization-dependent spectral shift can be masked or even reversed when the forming particles significantly deviate from sphericity (aspect ratio in the 1.2−1.3 range), due to competition between the effects of electromagnetic coupling of the Ag and Au particles in the dimer and of their individual shape anisotropy. The impact of particle coupling on the optical response of a heterodimer can thus be unambiguously investigated only if its morphology is independently determined.

The measured extinction cross-section amplitude, spectral shape, and polarization dependence were found to be in excellent agreement with FEM

numerical simulations using the size, shape, and orientation of the individual dimers determined by TEM. In particular, enhancement of the optical response around the gold-like LSPR due to interaction with the Ag particle is quantitatively reproduced, as well as the shape- and polarization-dependent spectral shift of the resonances. For quasispherical particles, the polarization dependence of the Ag-like LSPR wavelength is an indirect signature of the Fano resonance effect predicted theoretically in small gold—silver heterodimers. More generally, the observed spectral and amplitude behaviors of the optical response of a heterodimer are manifestations of local modification of the electromagnetic field distribution in and around the constituent particles. This opens many possibilities for nanoscale manipulation of the electromagnetic field playing with the constituent particle composition, size, shape, and coupling (*via* their separation).

METHODS

Chemicals. Ascorbic acid, tetraethylorthosilicate (TEOS), and ethylene glycol were supplied by Aldrich. Sodium citrate, tetrachloroauric acid trihydrate ($HAuCl_4 \times 3H_2O$), and cetyltrimethylammonium bromide (CTAB) were purchased from Sigma. Poly(allylamine hydrochloride) (PAH, M_w 15 000), sodium hydrosulfide (NaSH), poly(vinyl pyrrolidone) (PVP, M_w 55 000), silver trifluoroacetate (CF_3COOAg), and HCl solution were purchased from Aldrich. Dimethylamine solution (DMA) was supplied by Fluka. Pure-grade ethanol and Milli-Q-grade water were used in all preparations. All chemicals were used as received.

Synthesis of Au Spheres. Citrate-Au seeds (15 nm, [Au] = 3.56 × 10^{-6} M) were prepared by the standard Turkevich method.[47] A 2.5 mL amount of ascorbic acid (0.5 mM) was added to 500 mL of an aqueous solution containing $HAuCl_4$ (0.25 mM) and CTAB (0.015 M) at 35 °C. Subsequently, 7.5 mL of the seed solution was added and the growth reaction was allowed to proceed for one hour, to obtain gold nanospheres with an average diameter of 65 ± 5 nm, as determined from TEM images.[48] Prior to dimer formation, the gold spheres were coated with PVP by first centrifuging (8000 rpm, 20 min) and redispersing in Milli-Q water, followed by dropwise addition of a PVP aqueous solution, previously sonicated during 15 min ([Au]/[PVP] ratio = 1), under vigorous stirring. The mixture was gently stirred overnight and then centrifuged (3500 rpm, 3 h) and redispersed in ethanol under sonication.[49]

Silica Coating of Silver Nanoparticles and Amine Functionalization of Silica Shell Surface. PVP-stabilized silver nanoparticles were prepared by using a previously reported method.[26] Subsequently, silica coating was carried out by addition of a sol—gel precursor mixture to the silver colloid, with the following final concentrations: [Ag] = 0.1 mM; [H_2O] = 10.55 M; [DMA] = 0.016 M; [TEOS] = 0.8 mM.[27] The mixture was then centrifuged (2500 rpm, 30 min) twice and redispersed in ethanol. The synthesis yielded average sizes of 37 ± 2 nm for the silver core diameter and 16 ± 2 nm for the silica shell thickness. The silica shell surface was then modified with amino groups by mixing 4 mL of Ag@SiO_2 (0.2 mM) in ethanol with 4 mL of PAH (M_w 15 000, 0.8 mg/mL) aqueous solution and stirring overnight.[50] The mixture was centrifuged at 1200 rpm twice, and the precipitate redispersed in 8 mL of water so that the Ag concentration was around 0.1 mM.

Formation of Au—Ag@SiO_2 Dimers. In a typical experiment to prepare the hybrid nanostructures, 1 mL of Au@PVP in ethanol (0.233 mM) was added dropwise under vigorous stirring to 1 mL of AgNP@SiO_2@PAH (0.1 mM) in water. In order to allow electrostatic attachment of Au@PVP onto Ag NP@SiO_2PAH, the samples were allowed to mix for 2 h. Finally, the product was extensively diluted with milli-Q-water and spin-coated onto a 40 nm thick transparent silica membrane.

Absolute Extinction Cross-Section Measurements of Single Dimers. The light polarization dependent extinction cross-section spectrum of single dimers was measured using the spatial modulation spectroscopy technique.[31] The incident light beam was focused using a 100× microscope objective with a numerical aperture of 0.75, yielding focal spot sizes of $d \approx 0.7\lambda$ (full width at half-maximum of the light intensity profile). The sample position was modulated at $f \approx 1.5$ kHz. The light power transmitted through the sample was detected by an avalanche photodiode, and its $2f$ component was extracted by a lock-in amplifier.[29] The light source used in our experiments was a femtosecond optical parametric oscillator (OPO) pumped by a Ti:Sapphire oscillator. The OPO generates pulses tunable in the 490—690 nm wavelength range. The 400—490 nm spectral range was covered by frequency doubling in a BBO crystal with a tunable Ti:Sapphire oscillator. Combining these sources, wavelengths over the visible range 400—690 nm required for gold—silver heterodimer spectroscopy could be created.

Correlation of Optical Measurements with TEM Microscopy. To combine SMS and TEM characterizations of single nanodimers, colloidal dimer solutions were spin-coated on TEM grids with 50 × 50 μm^2 windows covered by a 40 nm thick silica film. Spin-coating conditions were adjusted so as to yield a > 1 μm average spacing between deposited nano-objects, compatible with their individual observation using optical means. Individual dimers were first localized on the surface by low-magnification (typically ×2000) TEM observation and distinguished from unpaired gold or silver nano-objects. Importantly, the moderate electron beam illuminations used for this nano-object selection step have been shown not to alter their optical properties.[35] The optical response of the selected dimers was subsequently measured by SMS. Finally, they were imaged with TEM using high magnifications (typically ×200 000) to precisely characterize their geometry.[32]

Finite-Element Modeling. Spherical geometries were used for gold and silver nanoparticles and silica shells (Figure 2d), unless specified. The silica substrate on which the dimers are deposited was modeled as a semi-infinite medium (taking into account its finite thickness yields identical results, as the substrate thickness is comparable to the sizes of the particles). A refractive index value of 1.45 was used for both the silica substrate and the silica shell, while the refractive index, n_m, of the surrounding medium in the half-space above the substrate is used as a free parameter to account for the possible presence of surfactant molecules or residual solvent (its value is typically here in the 1.2—1.3 range).[35] Absorption cross-sections were deduced from the spatial integral of resistive heating. Scattering cross-sections were deduced from the flux of the Poynting vector of the scattered electromagnetic field over a sphere surrounding the dimer.[35]

Conflict of Interest: The authors declare no competing financial interest.

Supporting Information Available: Modeling using a dipolar-quasistatic approach; dependence of heterodimer extinction on Au—Ag separation; elliptical nanoparticles: effect of orientation; heterodimers with complex morphologies; absorption and scattering cross-sections computed for the heterodimer of Figure 3a; spatial distribution of the total electric field in and around isolated Ag@SiO_2 and Au nanoparticles; quasistatic computations performed for incident light polarization orthogonal to the dimer axis. This material is available free of charge *via* the Internet at http://pubs.acs.org.

REFERENCES AND NOTES

1. Kelly, K. L.; Coronado, E.; Zhao, L. L.; Schatz, G. C. The Optical Properties of Metal Nanoparticles: The Influence of Size, Shape, and Dielectric Environment. *J. Phys. Chem. B* **2003**, *107*, 668–677.

2. Liz-Marzán, L. M. Tailoring Surface Plasmons through the Morphology and Assembly of Metal Nanoparticles. *Langmuir* **2006**, *22*, 32–41.

3. Romo-Herrera, J. M.; Alvarez-Puebla, R. A.; Liz-Marzán, L. M. Controlled Assembly of Plasmonic Colloidal Nanoparticle Clusters. *Nanoscale* **2011**, *3*, 1304–1315.

4. Halas, N. J.; Lal, S.; Chang, W.-S.; Link, S.; Nordlander, P. Plasmons in Strongly Coupled Metallic Nanostructures. *Chem. Rev.* **2011**, *111*, 3913–3961.

5. Su, K.-H.; Wei, Q.-H.; Zhang, X.; Mock, J. J.; Smith, D. R.; Schultz, S. Interparticle Coupling Effects on Plasmon Resonances of Nanogold Particles. *Nano Lett.* **2003**, *3*, 1087–1090.

6. Gunnarsson, L.; Rindzevicius, T.; Prikulis, J.; Kasemo, B.; Käll, M.; Zou, S.; Schatz, G. C. Confined Plasmons in Nanofabricated Single Silver Particle Pairs: Experimental Observations of Strong Interparticle Interactions. *J. Phys. Chem. B* **2005**, *109*, 1079–1087.

7. Reinhard, B. M.; Siu, M.; Agarwal, H.; Alivisatos, P.; Liphardt, J. Calibration of Dynamic Molecular Rulers Based on Plasmon Coupling between Gold Nanoparticles. *Nano Lett.* **2005**, *5*, 2246–2252.

8. Brown, L. V; Sobhani, H.; Lassiter, J. B.; Nordlander, P.; Halas, N. J. Heterodimers: Plasmonic Properties of Mismatched Nanoparticle Pairs. *ACS Nano* **2010**, *4*, 819–832.

9. Yang, L.; Wang, H.; Yan, B.; Reinhard, B. M. Calibration of Silver Plasmon Rulers in the 1−25 nm Separation Range: Experimental Indications of Distinct Plasmon Coupling Regimes. *J. Phys. Chem. C* **2010**, *114*, 4901–4908.

10. Sheikholeslami, S.; Jun, Y.; Jain, P. K.; Alivisatos, P. Coupling of Optical Resonances in a Compositionally Asymmetric Plasmonic Nanoparticle Dimer. *Nano Lett.* **2010**, *10*, 2655–2660.

11. Busson, M. P.; Rolly, B.; Stout, B.; Bonod, N.; Larquet, E.; Polman, A.; Bidault, S. Optical and Topological Characterization of Gold Nanoparticle Dimers Linked by a Single DNA Double Strand. *Nano Lett.* **2011**, *11*, 5060–5065.

12. Prodan, E.; Radloff, C.; Halas, N. J.; Nordlander, P. A Hybridization Model for the Plasmon Response of Complex Nanostructures. *Science* **2003**, *302*, 419–422.

13. Nordlander, P.; Oubre, C.; Prodan, E.; Li, K.; Stockman, M. I. Plasmon Hybridization in Nanoparticle Dimers. *Nano Lett.* **2004**, *4*, 899–903.

14. McMahon, J. M.; Henry, A.-I.; Wustholz, K. L.; Natan, M. J.; Freeman, R. G.; Van Duyne, R. P.; Schatz, G. C. Gold Nanoparticle Dimer Plasmonics: Finite Element Method Calculations of the Electromagnetic Enhancement to Surface-Enhanced Raman Spectroscopy. *Anal. Bioanal. Chem.* **2009**, *394*, 1819–1825.

15. Romero, I.; Aizpurua, J.; Bryant, G. W.; García De Abajo, F. J. Plasmons in Nearly Touching Metallic Nanoparticles: Singular Response in the Limit of Touching Dimers. *Opt. Express* **2006**, *14*, 9988–9999.

16. Hatab, N. A.; Hsueh, C.-H.; Gaddis, A. L.; Retterer, S. T.; Li, J.-H.; Eres, G.; Zhang, Z.; Gu, B. Free-Standing Optical Gold Bowtie Nanoantenna with Variable Gap Size for Enhanced Raman Spectroscopy. *Nano Lett.* **2010**, *10*, 4952–4955.

17. Ringler, M.; Schwemer, A.; Wunderlich, M.; Nichtl, A.; Kürzinger, K.; Klar, T.; Feldmann, J. Shaping Emission Spectra of Fluorescent Molecules with Single Plasmonic Nanoresonators. *Phys. Rev. Lett.* **2008**, *100*, 203002.

18. Jain, P. K.; El-Sayed, M. A. Noble Metal Nanoparticle Pairs: Effect of Medium for Enhanced Nanosensing. *Nano Lett.* **2008**, *8*, 4347–4352.

19. Aćimović, S. S.; Kreuzer, M. P.; González, M. U.; Quidant, R. Plasmon Near-Field Coupling in Metal Dimers as a Step Toward Single-Molecule Sensing. *ACS Nano* **2009**, *3*, 1231–1237.

20. Sönnichsen, C.; Reinhard, B. M.; Liphardt, J.; Alivisatos, A. P. A Molecular Ruler Based on Plasmon Coupling of Single Gold and Silver Nanoparticles. *Nat. Biotechnol.* **2005**, *23*, 741–745.

21. Jain, P. K.; Huang, W.; El-Sayed, M. A. On the Universal Scaling Behavior of the Distance Decay of Plasmon Coupling in Metal Nanoparticle Pairs: A Plasmon Ruler Equation. *Nano Lett.* **2007**, *7*, 2080–2088.

22. Bachelier, G.; Russier-Antoine, I.; Benichou, E.; Jonin, C.; Del Fatti, N.; Vallée, F.; Brevet, P.-F. Fano Profiles Induced by Near-Field Coupling in Heterogeneous Dimers of Gold and Silver Nanoparticles. *Phys. Rev. Lett.* **2008**, *101*, 197401.

23. Encina, E. R.; Coronado, E. A. On the Far Field Optical Properties of Ag−Au Nanosphere Pairs. *J. Phys. Chem. C* **2010**, *114*, 16278–16284.

24. Encina, E. R.; Coronado, E. A. Near Field Enhancement in Ag Au Nanospheres Heterodimers. *J. Phys. Chem. C* **2011**, *115*, 15908–15914.

25. Peña-Rodríguez, O.; Pal, U.; Campoy-Quiles, M.; Rodríguez-Fernández, L.; Garriga, M.; Alonso, M. I. Enhanced Fano Resonance in Asymmetrical Au:Ag Heterodimers. *J. Phys. Chem. C* **2011**, *115*, 6410–6414.

26. Zhang, Q.; Li, W.; Wen, L.-P.; Chen, J.; Xia, Y. Facile Synthesis of Ag Nanocubes of 30 to 70 nm in Edge Length with CF_3COOAg as a Precursor. *Chem. Eur. J.* **2010**, *16*, 10234–10239.

27. Kobayashi, Y.; Katakami, H.; Mine, E.; Nagao, D.; Konno, M.; Liz-Marzán, L. M. Silica Coating of Silver Nanoparticles Using a Modified Stöber Method. *J. Colloid Interface Sci.* **2005**, *283*, 392–396.

28. Muskens, O.; Christofilos, D.; Del Fatti, N.; Vallée, F. Optical Response of a Single Noble Metal Nanoparticle. *J. Opt. A: Pure Appl. Opt.* **2006**, *8*, S264–S272.

29. Muskens, O.; Billaud, P.; Broyer, M.; Del Fatti, N.; Vallée, F. Optical Extinction Spectrum of a Single Metal Nanoparticle: Quantitative Characterization of a Particle and of Its Local Environment. *Phys. Rev. B* **2008**, *78*, 205410.

30. Muskens, O. L.; Bachelier, G.; Del Fatti, N.; Vallée, F.; Brioude, A.; Jiang, X.; Pileni, M.-P. Quantitative Absorption Spectroscopy of a Single Gold Nanorod. *J. Phys. Chem. C* **2008**, *112*, 8917–8921.

31. Arbouet, A.; Christofilos, D.; Del Fatti, N.; Vallée, F.; Huntzinger, J.; Arnaud, L.; Billaud, P.; Broyer, M. Direct Measurement of the Single-Metal-Cluster Optical Absorption. *Phys. Rev. Lett.* **2004**, *93*, 127401.

32. Billaud, P.; Marhaba, S.; Cottancin, E.; Arnaud, L.; Bachelier, G.; Bonnet, C.; Del Fatti, N.; Lermé, J.; Vallée, F.; Vialle, J.-L. Correlation between the Extinction Spectrum of a Single Metal Nanoparticle and Its Electron Microscopy Image. *J. Phys. Chem. C* **2008**, *112*, 978–982.

33. Grillet, N.; Manchon, D.; Bertorelle, F.; Bonnet, C.; Broyer, M.; Cottancin, E.; Lermé, J.; Hillenkamp, M.; Pellarin, M. Plasmon Coupling in Silver Nanocube Dimers: Resonance Splitting Induced by Edge Rounding. *ACS Nano* **2011**, *5*, 9450–9462.

34. Davletshin, Y. R.; Lombardi, A.; Cardinal, M. F.; Juvé, V.; Crut, A.; Maioli, P.; Liz-Marzán, L. M.; Vallée, F.; Del Fatti, N.; Kumaradas, J. C. A Quantitative Study of the Environmental Effects on the Optical Response of Gold Nanorods. *ACS Nano* **2012**, *6*, 8183–8193.

35. Lombardi, A.; Loumaigne, M.; Crut, A.; Maioli, P.; Del Fatti, N.; Vallée, F.; Spuch-Calvar, M.; Burgin, J.; Majimel, J.; Tréguer-Delapierre, M. Surface Plasmon Resonance Properties of Single Elongated Nano-objects: Gold Nanobipyramids and Nanorods. *Langmuir* **2012**, *28*, 9027–9033.

36. Baida, H.; Billaud, P.; Marhaba, S.; Christofilos, D.; Cottancin, E.; Crut, A.; Lermé, J.; Maioli, P.; Pellarin, M.; Broyer, M.; *et al.* Quantitative Determination of the Size Dependence of Surface Plasmon Resonance Damping in Single Ag@SiO$_2$ Nanoparticles. *Nano Lett.* **2009**, *9*, 3463–3469.

37. Johnson, P. B.; Christy, R. W. Optical Constants of the Noble Metals. *Phys. Rev. B* **1972**, *6*, 4370–4379.

38. Palik, E. D. *Handbook of Optical Constants of Solids*; Academic Press: New York, 1985.

39. Billaud, P.; Huntzinger, J.-R.; Cottancin, E.; Lermé, J.; Pellarin, M.; Arnaud, L.; Broyer, M.; Del Fatti, N.; Vallée, F.

Optical Extinction Spectroscopy of Single Silver Nanoparticles. *Eur. Phys. J. D* **2007**, *43*, 271–274.

40. Liu, M.; Guyot-Sionnest, P. Preparation and Optical Properties of Silver Chalcogenide Coated Gold Nanorods. *J. Mater. Chem.* **2006**, *16*, 3942–3945.

41. Hartland, G. V. Optical Studies of Dynamics in Noble Metal Nanostructures. *Chem. Rev.* **2011**, *111*, 3858–3887.

42. Esteban, R.; Borisov, A. G.; Nordlander, P.; Aizpurua, J. Bridging Quantum and Classical Plasmonics with a Quantum-Corrected Model. *Nat. Commun.* **2012**, *3*, 825.

43. Liz-Marzán, L. M.; Giersig, M.; Mulvaney, P. Synthesis of Nanosized Gold-Silica Core-Shell Particles. *Langmuir* **1996**, *7463*, 4329–4335.

44. Li, J. F.; Huang, Y. F.; Ding, Y.; Yang, Z. L.; Li, S. B.; Zhou, X. S.; Fan, F. R.; Zhang, W.; Zhou, Z. Y.; Wu, D. Y.; *et al.* Shell-Isolated Nanoparticle-Enhanced Raman Spectroscopy. *Nature* **2010**, *464*, 392–395.

45. Ersen, O.; Hirlimann, C.; Drillon, M.; Werckmann, J.; Tihay, F.; Pham-Huu, C.; Crucifix, C.; Schultz, P. 3D-TEM Characterization of Nanometric Objects. *Solid State Sci.* **2007**, *9*, 1088–1098.

46. Goris, B.; Bals, S.; Van den Broek, W.; Carbó-Argibay, E.; Gómez-Graña, S.; Liz-Marzán, L. M.; Van Tendeloo, G. Atomic-Scale Determination of Surface Facets in Gold Nanorods. *Nat. Mater.* **2012**, *11*, 930–935.

47. Turkevich, J.; Stevenson, P. C.; Hillier, J. The Formation of Colloidal Gold. *J. Phys. Chem.* **1953**, *57*, 670–673.

48. Rodríguez-Fernández, J.; Pérez-Juste, J.; García de Abajo, F. J.; Liz-Marzán, L. M. Seeded Growth of Submicron Au Colloids with Quadrupole Plasmon Resonance Modes. *Langmuir* **2006**, *22*, 7007–7010.

49. Vial, S.; Pastoriza-Santos, I.; Pérez-Juste, J.; Liz-Marzán, L. M. Plasmon Coupling in Layer-by-Layer Assembled Gold Nanorod Films. *Langmuir* **2007**, *23*, 4606–4611.

50. Pastoriza-Santos, I.; Gomez, D.; Pérez-Juste, J.; Liz-Marzán, L. M.; Mulvaney, P. Optical Properties of Metal Nanoparticle Coated Silica Spheres: A Simple Effective Medium Approach. *Phys. Chem. Chem. Phys.* **2004**, *6*, 5056–5060.